JOURNAL OF BIOMEDICAL OPTICS 4(1), 183–190 (JANUARY 1999)

TIME INTEGRATED SPECTROSCOPY OF TURBID MEDIA BASED ON THE MICROSCOPIC BEER–LAMBERT LAW: APPLICATION TO SMALL-SIZE PHANTOMS HAVING DIFFERENT BOUNDARY CONDITIONS

Hedong Zhang,[†] Tsuneyuki Urakami,[‡] Yutaka Tsuchiya,[‡] Zukang Lu,[†] and Teruo Hiruma[‡]
[†]Zhejiang University, State Key Laboratory of Modern Optical Instrumentation, Hangzhou, 310027, People's Republic of China; [‡]Central Research Laboratory, Hamamatsu Photonics K.K., 5000 Hirakuchi, Hamakita 434-8601, Japan

(Paper CDO-011 received May 28, 1998; revised manuscript received Nov. 18, 1998; accepted for publication Nov. 19, 1998.)

ABSTRACT

Continued work on time-integrated spectroscopy (TIS) is presented to quantify absorber concentrations in turbid media. We investigated the applicability of the TIS method to small-size media that have different boundary conditions by measuring two $20\times20\times50\,\mathrm{mm}^3$ cuboid liquid tissue-like phantoms at various absorption levels (absorption coefficients of the phantom from 2.5×10^{-3} to $4.4\times10^{-2}\,\mathrm{mm}^{-1}$ at 782 nm and from 3.1×10^{-3} to $2.7\times10^{-2}\,\mathrm{mm}^{-1}$ at 831 nm). The scattering and absorbing solution was filled into ordinary and black-anodized aluminum containers to provide different boundary conditions. By means of a single equation, the absorber concentrations have been recovered within errors of a few percent in both cases. This demonstrates that the TIS method can quantify absorbers in small-size media having different boundary conditions. © *1999 Society of Photo-Optical Instrumentation Engineers.* [S1083-3668(99)01101-6]

Keywords tissue spectroscopy; time integrated spectroscopy; small-size media; boundary conditions.

1 INTRODUCTION

The measurement of optical properties, i.e., the absorption coefficient μ_a and the reduced scattering coefficient μ_s', of biological tissues is attracting great interest in the biomedical field.[1] Knowledge of these parameters provides important information, such as the metabolism and health status of living tissues, for both diagnostic and therapeutic applications. Up to now, a variety of methods have been developed for this purpose. Among them, methods based on the photon diffusion equation have been widely applied to measure tissues and tissue-like phantoms, allowing the estimation of μ_a and μ_s' from highly scattering media.[2–5] However, due to inherent flaws in the photon diffusion theory, these methods encounter the following problems during practical applications. First, the photon diffusion equation treats the reduced scattering coefficient μ_s' and is therefore only valid in relatively large media in which enough scattering events occur so that photons lose their initial directionality.[6] Second, in the derivation of the photon diffusion equation, one has to incorporate exact descriptions of boundary conditions, such as zero- or extrapolated- index matched or mismatched-boundary conditions and exterior shapes of target media. Application of the photon diffusion equation is therefore restricted to media that have simple shapes.[7] Many results show that significant errors can occur if the effect of the refractive index mismatched boundary is not properly taken into account.[8–10] The errors are more important when reemission from small-size media are measured, because the influence of the boundary increases as the size of media decreases. These problems thus challenge us to develop a new method for noninvasively quantifying optical parameters in small-size media having different boundary conditions.

The methods based on the microscopic Beer–Lambert law (MBL), which describes the survival probability of a photon by its zigzag path within the medium, are very simple and implicit for boundary conditions, exterior shapes, and source-detector separation. In the case of the MBL, the effects of scattering and absorbing are separated and a simple relation can be obtained between absorption coefficient and observables such as attenuation

Address all correspondence to Yutaka Tsuchiya. E-mail: tsuchy@crl.hpk.co.jp

and path length. But the methods based on the MBL are usually unable to quantify scattering properties since the MBL lacks explicit analytic expressions to describe scattering events. However, when we consider the applications to monitor blood oxygenation[3,11–14] and dosimetry during photodynamic therapy (PDT) of cancer,[15,16] it is important to measure μ_a but not μ_s' of the tissue, because the optical absorption in tissue is indicative of the concentration of chromophores such as hemoglobin and PDT photosensitizers. From this viewpoint, the time integrated spectroscopy (TIS) method[17–19] that Tsuchiya and Urakami originally proposed based on the MBL might be a better choice because of its high accuracy and flexibility.

In those original articles, it has been theoretically shown that the TIS method derived from the MBL can quantify absorbing substances in highly scattering media, regardless of the system size and exterior shape, the refractive-index matched or mismatched boundary conditions, source–detector separations, and measuring schemes such as transmission or reflection detection. Zhang et al. first demonstrated the validity of the TIS method by measuring tissue-like phantoms[20] and improved the accuracy of the TIS method by deriving a more rigorous equation involving the wavelength dependence of scattering properties.[21] The TIS method has also been experimentally demonstrated to be independent of source–detector separations and measuring schemes,[20,21] and has been successfully applied to finite media with curved boundary.[22]

In this article, we present continued work on the TIS method. We investigate the applicability of the TIS method to small-size media having different boundary conditions by measurement of transmission from two $20\times20\times50\,\mathrm{mm}^3$ cuboid liquid tissue-like phantoms at various absorption levels. The scattering and absorbing solution, of which the phantoms are composed, was filled into ordinary and black-anodized aluminum containers to provide different boundary conditions.

2 THEORETICAL MODEL

Only a brief description of the TIS method will be given here. For a full understanding of this method, one should refer to the original papers by Tsuchiya and Urakami[18,19] and Zhang et al.[20,21]

First, we consider dual-wavelength spectroscopy of a homogeneous scattering medium that contains an absorber. The two wavelengths are denoted by λ_1 and λ_2, where the scattering coefficients are $\mu_s = \mu_{s1}$ and μ_{s2}, and the reduced scattering coefficients are $\mu_s' = \mu_{s1}'$ and μ_{s2}', respectively. The absorption coefficients at the respective wavelengths are expressed by

$$\mu_{a1} = C\epsilon_1 + \mu_{w1}, \quad \mu_{a2} = C\epsilon_2 + \mu_{w2}, \tag{1}$$

where C is the concentration of the absorber, ϵ_1 and ϵ_2 are the extinction coefficients of the absorber, and μ_{w1} and μ_{w2} are the absorption coefficients of water at the respective wavelengths λ_1 and λ_2. The concentration C in Eq. (1) is the quantity of interest in the dual-wavelength TIS method.

According to the MBL, photon intensity $I(\mu_s, \mu_a)$, i.e., the temporal integration of the impulse response of a turbid medium satisfies

$$\ln I(\mu_s, \mu_a) = -\int_0^{\mu_a} L(\mu_s, \mu_a)\, d\mu_a + \ln \int_0^{\infty} s(\mu_s, t)\, dt, \tag{2}$$

where the term $s(\mu_s, t)$ represents the probability of scattered photons that reach the detector in the absence of absorption, and $L(\mu_s, \mu_a)$ denotes the mean path length traveled by photons in the medium and can be determined from the time-resolved profile of re-emission and the impulse response of measuring system by the simple subtraction[23] or deconvolution method.

During the practical measurement it is usually inevitable that the sensitivity of measuring system depends on wavelength. We have therefore introduced a factor b which is the ratio of the sensitivities of the measuring system at the respective wavelengths. The relation between $I(\mu_{s1}, \mu_{a1})$ and $I(\mu_{s2}, \mu_{a2})$ is thus expressed as

$$\ln \frac{I(\mu_{s1}, \mu_{a1})}{bkI(\mu_{s2}, \mu_{a2})} = -\int_0^{\mu_{a1}} L(\mu_{s1}, \mu_a)\, d\mu_a + \int_0^{\mu_{a2}} L(\mu_{s2}, \mu_a)\, d\mu_a, \tag{3a}$$

$$k \equiv \int_0^{\infty} s(\mu_{s1}, t)\, dt \Big/ \int_0^{\infty} s(\mu_{s2}, t)\, dt, \tag{3b}$$

where k is used to incorporate the wavelength dependence of the photon intensity, i.e., the difference in photon intensities at the respective wavelengths due to wavelength dependent scattering properties and boundary conditions. Furthermore, in the case of relatively large and simple shape media, the factor k is derived from the steady state diffusion solution at $\mu_a = 0$ as

$$k \approx \mu_{s2}' / \mu_{s1}'. \tag{3c}$$

Combining Eqs. (1) and (3) and applying the mean value theorem, we finally obtain the concentration of the absorber as

$$C=\frac{\ln\dfrac{I(\mu_{s1},\mu_{a1})}{bkI(\mu_{s2},\mu_{a2})}-\mu_{w1}L(\mu_{s1},\mu_{a1})(k'-1)-(\mu_{w2}-\mu_{w1})\dfrac{L(\mu_{s1},\mu_{a1})k'+L(\mu_{s2},\mu_{a2})}{2}}{\epsilon_1 L(\mu_{s1},\mu_{a1})(k'-1)+(\epsilon_2-\epsilon_1)\dfrac{L(\mu_{s1},\mu_{a1})k'+L(\mu_{s2},\mu_{a2})}{2}}, \tag{4a}$$

$$k'\equiv L(\mu_{s2},\mu_a)/L(\mu_{s1},\mu_a), \tag{4b}$$

where the factor k' is used to incorporate the wavelength dependence of mean path length. In other words, the difference in the photon-path distribution at the two wavelengths due to the wavelength dependent scattering properties and boundary conditions is taken into account in Eq. (4a). An approximation of the factor k' is derived for a semi-infinite medium based on the solution of photon diffusion equation as

$$k'\approx\sqrt{\mu'_{s2}/\mu'_{s1}}. \tag{4c}$$

This relation holds true for a source–detector separation much larger than $1/\mu'_s$ (for example, >30 mm) and optical properties typically found in biological samples.[21] Additionally, during the derivation of Eq. (4a), we have assumed that the difference between $L(\mu_{s2},\mu_a)$ and $L(\mu_{s1},\mu_a)$ is constant for μ_a in the range from 0 to $\min(\mu_{a1},\mu_{a2})$. This assumption is acceptable since $k'\approx 1$.

In practical dual-wavelength spectroscopy, we cannot directly obtain the values of k and k' according to their definition in Eqs. (3b) and (4b), because the photon intensity at $\mu_a=0$ is not measurable and the absorption coefficients of the medium are usually different at the two wavelengths. However, Eqs. (3c) and (4c) provide approximations of k and k' only if the ratio of the reduced scattering coefficients at the two wavelengths is known. Here, we should note that these approximations have been made based on the photon diffusion equation. Consequently, whether they are valid or not for small-size media is also a subject of interest in this study.

3 EXPERIMENTAL SETUP

The experimental setup has been illustrated and described in detail elsewhere.[4,23] Here only the tissue-like phantom is schematically shown in Figure 1 with photon incident and detection sites. Laser diode pulses (Hamamatsu, PLP) of 782 and 831 nm alternatively passed through a neutral density attenuator were coupled into a 200 μm-diam graded index optical fiber in contact with the tissue-like phantom through a glass window. Other parameters of laser pulses are 50 ps full width at half maximum (FWHM) in duration, 5 MHz repetition rate, and 100 mW peak power at the output end of the fiber. The diffusely transmitted photons were collected at the center of the opposite surface of the phantom by a 5-mm-diam optical bundle fiber through a glass window and fed into a time-correlated single photon counting system (TCSPC). The signals from the TCSPC system were then digitized by an analog-to-digital (A/D) converter, accumulated in the memory of a personal computer, thus obtaining a temporal profile of the transmission. Additionally, in order to obtain the parameter b and to determine the mean pathlength which are essential for the analysis, the impulse responses of the whole measuring system (i.e., the instrumental function) at the two wavelengths were also measured by making the source and detector fibers abut one another.

The tissue-like phantoms were composed of 1% Intralipid-20% (Pharmacia AB, Stockholm) that served as scatterers and greenish-brown ink (Chugai Kasei, Mitaka-City) that acted as a pure absorber in the range of our experiment.[19] Greenish-brown ink was added into the Intralipid suspension of 1000 ml in 0.2 ml steps until the total volume of the ink reached 2.0 ml, so that the absorption was changed independently. An appropriate volume of the solution including different volumes of ink was filled into a small aluminum container ($20\times 20\times 50$ mm^3, hereafter simply referred to as container 1). The top surface of the solution was 45 mm from

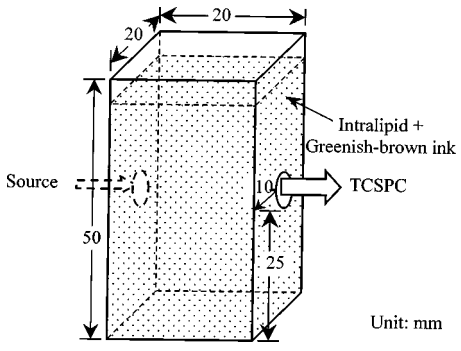

Fig. 1 Tissue-like phantom with photon incident and detection sites. The tissue-like phantoms were composed of 1% Intralipid-20% suspension as a scattering substance and greenish-brown ink as a pure absorber. An appropriate volume of the solution with ink of different volumes was filled into a small aluminum container and a black-anodized aluminum container ($20\times 20\times 50$ mm^3). The top surface of the solution was 45 mm from the bottom of the container. Light pulses of 782 and 831 nm alternatively illuminated the phantom through a glass window. The diffusely transmitted photons were collected through a glass window at the center of the opposite surface of the phantom by an optical bundle fiber and fed into a time-correlated single photon counting system (TCSPC).

the bottom of the container. The same experiment was repeated with a black-anodized aluminum container ($20\times20\times50\,mm^3$, hereafter simply referred to as container 2) in order to investigate the influence of boundary conditions. Photons that reached the internal surface were highly reflected in container 1 due to the aluminum reflective surface, while photons were highly absorbed in container 2.

In order to obtain approximate values for k and k', we estimated the reduced scattering coefficients of the Intralipid suspension, in a manner similar to that of van Staveren et al.,[24] to be 1.02 and $0.953\,mm^{-1}$ at 782 and 831 nm, respectively. The factors k and k' were thus calculated to be 1.070 and 1.035 by Eqs. (3c) and (4c), respectively. The method of van Staveren may contain some errors in determining the absolute value of μ_s'. However, it has been shown that the ratio of μ_s' at different wavelengths (i.e., the wavelength dependence of μ_s') agrees well with that determined by fitting the reflectance from a semi-infinite phantom with the photon diffusion equation.[25] Use of values k and k' is therefore justifiable in our analyses.

The absorption coefficients of greenish-brown ink were determined through calibration measurements of various concentrations of the ink in distilled water by a spectrophotometer. These values, along with the absorption of water measured by a spectrophotometer ($2.5\times10^{-3}\,mm^{-1}$ at 782 nm and $3.1\times10^{-3}\,mm^{-1}$ at 831 nm), yielded absorption coefficients for the phantom in a range from 2.5×10^{-3} to $4.4\times10^{-2}\,mm^{-1}$ at 782 nm, and from 3.1×10^{-3} to $2.7\times10^{-2}\,mm^{-1}$ at 831 nm. These ranges cover the typical values of absorption in human tissues, for example, when absorption in forearm is considered. In addition, as we can see in Figures 2 and 3 shown later, there is about a 1% difference between the absorption coefficients in the experiments with containers 1 and 2, even though we used the same ink concentrations. This difference may result from certain error occurred during the calibration measurement and is small enough to be neglected in our further discussion.

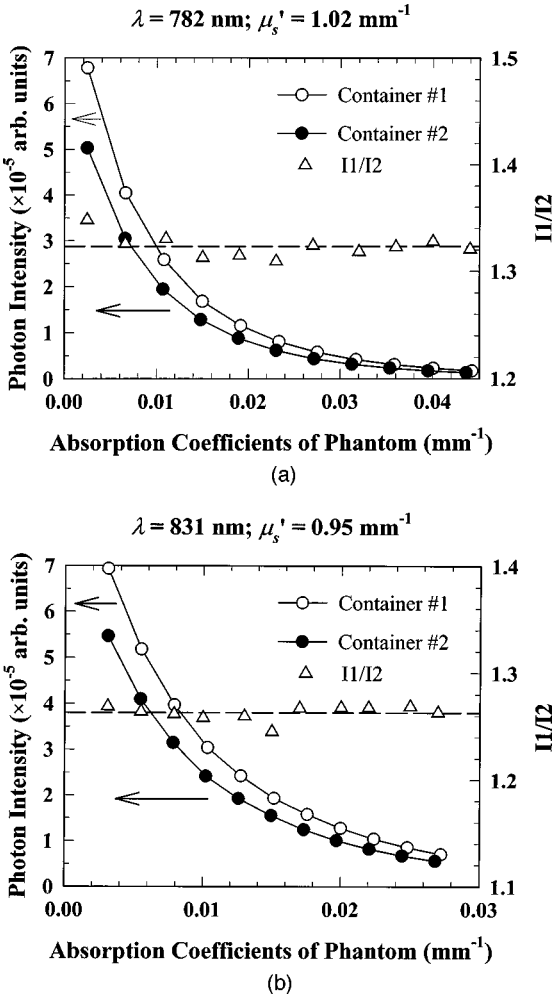

Fig. 2 Photon intensities measured using the containers 1 and 2 and their ratios at various absorption levels; (a) at 782 nm ($\mu_s' = 1.02\,mm^{-1}$), and (b) at 831 nm ($\mu_s' = 0.95\,mm^{-1}$). The broken lines are the average values of the photon intensity ratios measured using the two containers.

4 RESULTS

4.1 PHOTON INTENSITIES MEASURED USING DIFFERENT CONTAINERS

The photon intensities measured using the respective containers, as well as their ratios, are plotted versus absorption coefficients of the phantom in Figure 2; (a) at 782 nm ($\mu_s' = 1.02\,mm^{-1}$) and (b) at 831 nm ($\mu_s' = 0.95\,mm^{-1}$). Here the photon intensity is normalized by the quantity of incident light, so that the ordinate corresponds to the attenuation of the system. The photon intensity decreases rapidly as the absorption coefficient increases. However, the photon intensity at high absorption level still has enough signal-to-noise ratio. In addition, we can increase the intensity of incident light appropriately, if needed. We can see that the photon intensities measured using the container 1 are always higher than those with the container 2 at various absorption levels. This phenomenon is exclusively attributed to the different boundary conditions, i.e., reflection at the internal surface of container 1, while absorption at the internal surface of container 2.

In either Figure 2(a) or 2(b), the ratios of the respective photon intensities measured using the containers 1 and 2 are nearly constant in spite of the change in absorption coefficients of the phantoms. The ratios are calculated to be 1.32 ± 0.01 at 782 nm and 1.26 ± 0.01 at 831 nm. Comparing Figures 2(a) and 2(b), we see that the only difference lies in the wavelengths of the light sources. The discrepancy between the two ratios therefore indicates the influence of wavelength-dependent parameters: scattering properties and boundary conditions. In other

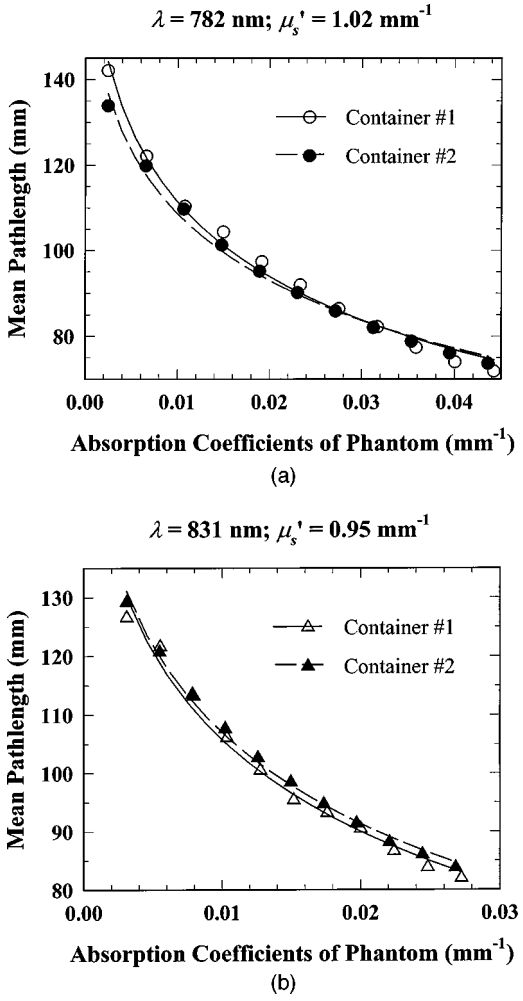

Fig. 3 Mean path lengths measured using the containers 1 and 2 at various absorption levels; (a) at 782 nm ($\mu_s' = 1.02\ \text{mm}^{-1}$), and (b) at 831 nm ($\mu_s' = 0.95\ \text{mm}^{-1}$). The smooth lines are obtained by fitting the experimental data shown by symbols with the equation $L = 1/(a + b\sqrt{\mu_a})$.

words, a different wavelength of incident light results in different scattering properties and different reflectance and absorbance at the internal surface of the boundary, and hence the different ratios mentioned above.

4.2 MEAN PATH LENGTH MEASURED USING DIFFERENT CONTAINERS

Similarly, the mean path lengths measured using the respective containers are plotted in Figure 3; (a) at 782 and (b) at 831 nm. The smooth lines are obtained by fitting the experimental data shown by symbols with the equation $L = 1/(a + b\sqrt{\mu_a})$, which is similar to the expression of the mean path length traveled by photons in a semi-infinite turbid medium.[7]

In Figures 3(a) and 3(b), there is no obvious difference between the mean path lengths traveled by photons in the phantoms having different boundary conditions. In Figure 3(a), the mean path lengths measured using the container 1 are a little larger than those with the container 2, and this tendency becomes smaller with an increase in μ_a. While in Figure 3(b), the mean path lengths measured using the container 2 are larger than those with the container 1, and this tendency becomes more obvious with an increase in μ_a. This different tendency may also be interpreted by the wavelength dependence of the scattering properties and boundary conditions. Further discussion will be given in Sec. 5 by referring to the temporal profile of the impulse response.

4.3 ABSORBER VOLUMES MEASURED BY DUAL-WAVELENGTH TIS METHOD

The volumes of ink were calculated by Eq. (4a), where the values of k and k' were estimated according to Eqs. (3c) and (4c), i.e., 1.070 and 1.035, respectively. The ink volumes measured using container 1 were plotted versus the added ink volumes in Figure 4(a) as well as the corresponding difference in absorption coefficients of the ink at 782 and 831 nm. The closed circles represent experimental results calculated with Eq. (4a) and the solid line shows the least-square fit which has a slope of 0.956 and y intercept of 0.020 ml. The theoretical values are also plotted with dotted lines as a reference. The y intercept value indicates the offset due to systematic error in the measurement. This offset may result from inaccuracy in approximating the factors k and k' and determining the absorption coefficients of water and zero point on the time axis.

In a similar manner as above, the results measured using the container 2 are shown in Figure 4(b). All the symbols and lines are the same as in Figure 4(a). The least-square fitting line has a slope of 0.952 and y intercept of 0.075 ml.

In both Figures 4(a) and 4(b), we see a good agreement between experimental results and theoretical values especially at the slopes. Here one should note that the ink volumes in the two different containers were accurately obtained by using the single equation, Eq. (4a). This strongly demonstrates the applicability of the TIS method to small-size media that have different boundary conditions.

5 DISCUSSION

5.1 INFLUENCE OF DIFFERENT BOUNDARY CONDITIONS

In dual-wavelength spectroscopy of small-size media, the influence of the boundary conditions on measured quantities is somewhat complex. The differences seen in each set of data in Figures 2(a)–3(b) indicate the influence of the boundary conditions on the photon intensity or the mean path length at the respective wavelengths. As seen in Figures 2 and 3, the different boundary conditions strongly affect the measured intensity, while almost no obvious influence can be observed on the mean path

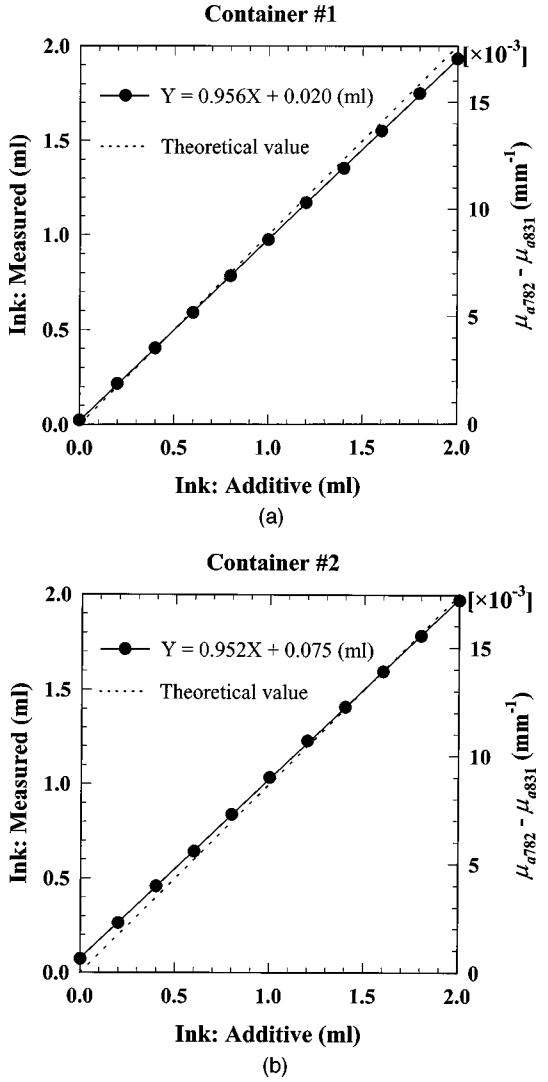

Fig. 4 Measured ink volumes as well as their corresponding difference in absorption coefficients of ink at 782 and 831 nm are plotted vs the additive ink volumes; (a) with container 1, and (b) with container 2. The closed circles represent experimental results calculated with Eq. (4a) and the solid lines show the least-square fits. The theoretical values are also plotted with dotted lines as a reference.

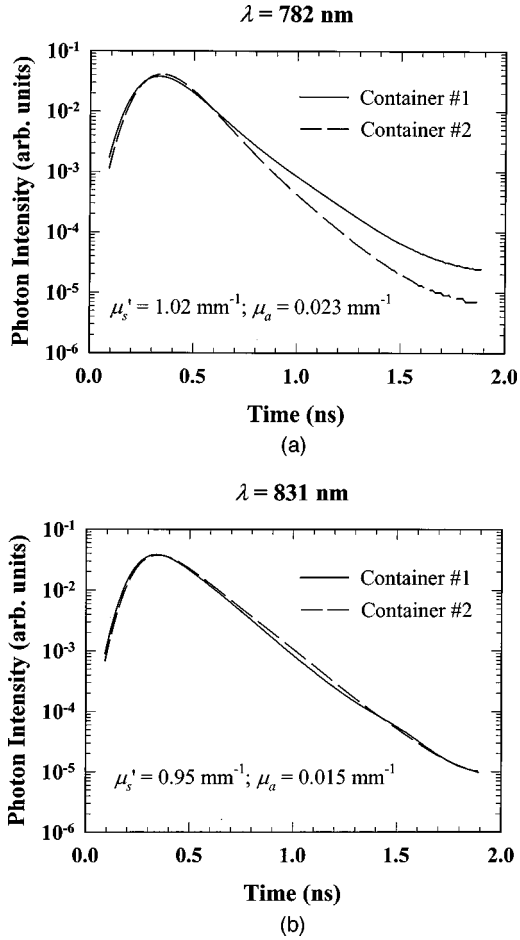

Fig. 5 Examples of impulse response (normalized by the total photon count) measured using the containers 1 and 2; (a) at 782 nm ($\mu_s' = 1.02\ \text{mm}^{-1}$, $\mu_a = 0.023\ \text{mm}^{-1}$); and (b) at 831 nm ($\mu_s' = 0.95\ \text{mm}^{-1}$, $\mu_a = 0.015\ \text{mm}^{-1}$). The solid and broken lines denote the impulse responses measured with containers 1 and 2, respectively.

length. The former can easily be interpreted by taking the different reflective and absorptive properties at different boundaries into account, but the latter is complicated. In order to understand these phenomena more clearly, we have investigated the temporal profiles of the impulse response measured using the containers 1 and 2 at each wavelength.

Examples of the impulse response are shown in Figure 5: (a) at 782 and (b) at 831 nm. Here the impulse responses have been normalized by the total counts of detected photons. The solid and broken lines denote the impulse responses measured using the containers 1 and 2, respectively. The optical properties of the phantom at the measurement were $\mu_a = 0.023\ \text{mm}^{-1}$ and $\mu_s' = 1.02\ \text{mm}^{-1}$ at 782 nm, and $\mu_a = 0.015\ \text{mm}^{-1}$ and $\mu_s' = 0.95\ \text{mm}^{-1}$ at 831 nm. These absorption levels correspond to the additive ink volume of 1.0 ml in the scattering media.

Since the photon intensities are shown in logarithmic scale in Figure 5, the difference in the mean path lengths (i.e., the centers of gravity of all the profiles in Figure 5) is exaggerated in visual sense. In fact, just as seen in Figures 3(a) and 3(b), we respectively obtained nearly the same mean path lengths for the profiles in Figures 5(a) and 5(b). In Figure 5(b), the profile measured using the container 2, compared to that with the container 1, has a small shift along the positive direction of the time axis. The small differences in the mean path lengths shown in Figure 3(b) correspond to this small shift of temporal profile (a shift of 10 ps corresponds to 2.26 mm change in the mean path length).

The two profiles shown in Figure 5(a) are obtained at the same absorption and scattering levels. However, a big difference in the decaying slopes of the profiles can be observed. This indicates that, in order to accurately determine the optical parameters from both of the profiles, we have to incorpo-

Table 1 Quantitation accuracy and the factors k and k'. Symbols Y and X are the same as in Figure 4.

Incorporated factors	Container 1 (ml)	Container 2 (ml)
$k=1.070$ & $k'=1.035$	$Y=0.956X+0.020$	$Y=0.952X+0.075$
$k=1.070$ & $k'=1$	$Y=1.024X+0.030$	$Y=1.018X+0.090$
$k=1$ & $k'=1$	$Y=1.045X+0.090$	$Y=1.038X+0.153$

rate the index-matched or mismatched boundary conditions in the diffusion model that is conventionally used to perform curve-fitting procedure.

In contrast, by using a single equation, we have obtained almost the same results from measurements with containers 1 and 2. The MBL itself is implicit for the boundary conditions and scattering properties because their influence is included in the observables; mean path length and photon intensity. Additionally the wavelength-dependent scattering properties and boundary conditions have been taken into consideration by introducing factors k and k' defined by Eqs. (3b) and (4b), respectively.

5.2 INFLUENCE OF WAVELENGTH DEPENDENCE OF BOUNDARY CONDITIONS

The relations between the two data in Figures 2(a) and 2(b), and Figures 3(a) and 3(b) are different. We can thus conclude that the two different boundaries have different wavelength dependent properties in our experiment. The wavelength dependence of both scattering properties and boundary conditions has been incorporated in Eq. (4a), so that we should have different values of k and k' in the experiments with containers 1 and 2. However, we simply used the same values of factors k and k' respectively estimated from Eqs. (3c) and (4c) in our analyses; that is to say, the wavelength dependence of boundary conditions was neglected in our case. Even so we still have obtained almost the same results especially at the slopes in both experiments as seen in Figure 4. This means that, in the case of our algorithm, the wavelength dependence of boundary conditions is not significant for determining the absorber concentrations.

5.3 INFLUENCE OF WAVELENGTH DEPENDENCE OF SCATTERING PROPERTIES

In theory, if we can accurately estimate the factors k and k' from Eqs. (3b) and (4b), we will obtain more accurate results. However, due to the reasons described previously, we can only estimate factors k and k' according to Eqs. (3c) and (4c), respectively. These equations have been derived based on the photon diffusion equation for a semi-infinite medium at a relatively large source–detector separation (>30 mm). The validity of Eqs. (3c) and (4c) was proven by measuring a finite medium.[22] However it is still unclear whether Eqs. (3c) and (4c) are applicable to small-size media or not.

To investigate the above point, we recalculated the absorber concentrations in a similar manner as before, but using different values for k and k'. The results are summarized in Table 1. When we set $k=k'=1$, the wavelength dependence of the scattering and boundary properties is disregarded. Comparing with the results obtained using $k=1.070$ and $k'=1.035$, we can observe almost the same accuracy in the slope (about $\pm 4\%$), but some improvement in the y intercept. Considering both slope and y intercept, use of $k=1.070$ and $k'=1.035$ yielded the closest values to the theoretical values. This indicates that approximations by Eqs. (3c) and (4c) are still acceptable in the case of small-size media.

6 CONCLUSION

The applicability of the dual-wavelength TIS method to small-size media that have different boundary conditions was investigated by measuring two $20\times20\times50\,\mathrm{mm}^3$ cuboid liquid tissue-like phantoms at various absorption levels. The different boundary conditions were obtained by filling the absorbing and scattering solution into ordinary and black-anodized aluminum containers. In both cases, the absorber concentrations were successfully recovered within errors of a few percent by using a single equation. This strongly demonstrates that the TIS method is applicable to small-size media that have different boundary conditions.

Acknowledgment

The authors are grateful to M. Miwa and Y. Yamashita for their useful discussions and technical support.

REFERENCES

1. See, for example, *OSA Tops. Adv. Opt. Imaging Photon Migration* **2** (1996).
2. M. S. Patterson, B. Chance, and B. C. Wilson, "Time resolved reflectance and transmittance for the noninvasive measurement of tissue optical properties," *Appl. Opt.* **28**(12), 2331–2336 (1989).
3. E. M. Sevick, B. Chance, J. Leigh, S. Nioka, and M. Maris, "Quantitation of time and frequency-resolved optical spectra for the determination of tissue oxygenation," *Anal. Biochem.* **195**, 330–351 (1991).
4. M. Miwa, Y. Ueda, and B. Chance, "Development of time resolved spectroscopy system for quantitative noninvasive

tissue measurement,'' *Proc. SPIE* **2389**, 142–149 (1995).
5. Y. Yamashita, M. Oda, H. Naruse, and M. Tamura, ''*In vivo* measurement of reduced scattering and absorption coefficients of living tissue using time-resolved spectroscopy,'' *OSA Tops. Adv. Opt. Imaging Photon Migration* **2**, 387–390 (1996).
6. K. M. Yoo, F. Liu, and R. R. Alfano, ''When does the diffusion approximation fail to describe photon transport in random media?'' *Phys. Rev. Lett.* **64**(22), 2647–2650 (1990); **65**(17), 2210–2211 (1990).
7. S. R. Arridge, M. Cope, and D. T. Delpy, ''The theoretical basis for the determination of optical pathlengths in tissue: temporal and frequency analysis,'' *Phys. Med. Biol.* **37**(7), 1531–1560 (1992).
8. R. C. Haskell, L. O. Svaasand, T. T. Tsay, T. C. Feng, M. S. McAdams, and B. J. Tromberg, ''Boundary conditions for the diffusion equation in radiative transfer,'' *J. Opt. Soc. Am. A* **11**(10), 2727–2741 (1994).
9. D. Contini, F. Martelli, and G. Zaccanti, ''Photon migration through a turbid slab described by a model based on diffusion approximation. I. Theory,'' *Appl. Opt.* **36**(19), 4587–4599 (1997).
10. F. Martelli, D. Contini, A. Taddeucci, and G. Zaccanti, ''Photon migration through a turbid slab described by a model based on diffusion approximation. II. Comparison with Monte Carlo results,'' *Appl. Opt.* **36**(19), 4600–4612 (1997).
11. F. F. Jöbsis, ''Noninvasive infrared monitoring of cerebral and myocardial oxygen sufficiency and circulatory parameters,'' *Science* **198**, 1264–1267 (1977).
12. M. Cope and D. T. Delpy, ''System for long-term measurement of cerebral blood and tissue oxygenation on newborn infants by near infrared transillumination,'' *Med. Biol. Eng. Comput.* **26**, 289–294 (1988).
13. B. Chance, S. Nioka, J. Kent, K. Mccully, M. Fountain, R. Greenfield, and G. Holtom, ''Time-resolved spectroscopy of haemoglobin in resting and ischemic muscles'' *Anal. Biochem.* **174**, 698–707 (1988).
14. M. Ferrari, Q. Wei, L. Carraresi, R. De Blasi, and G. Zaccanti, ''Time-resolved spectroscopy of the human forearm,'' *J. Photochem. Photobiol., B* **16**, 141–153 (1992).
15. B. C. Wilson, T. Farrell, and M. S. Patterson, ''An optical fiber-based diffuse reflectance spectrometer for noninvasive investigation of photodynamic sensitizers,'' in *In vivo Future Directions and Applications in Photodynamic Therapy,* SPIE Inst. Series Vol. S16, pp. 219–232, SPIE, Bellingham, WA (1990).
16. M. S. Patterson, J. D. Moulton, B. C. Wilson, and B. Chance, ''Applications of time-resolved light scattering measurements to photodynamic therapy dosimetry,'' *Proc. SPIE* **1203**, 62–74 (1990).
17. Y. Tsuchiya and T. Urakami, ''Photon migration model for turbid biological medium having various shapes,'' *Jpn. J. Appl. Phys., Part 2* **34**(1A), L79–81 (1995).
18. Y. Tsuchiya and T. Urakami, ''Noninvasive spectroscopy of variously shaped turbid media like human tissue based on the microscopic Beer-Lambert law,'' *OSA Tops. Adv. Opt. Imaging Photon Migration* **2**, 113–115 (1996).
19. Y. Tsuchiya and T. Urakami, ''Quantitation of absorbing substances in turbid media such as human tissues based on the microscopic Beer-Lambert law,'' *Opt. Commun.* **144**, 269–280 (1997).
20. H. Zhang, M. Miwa, Y. Yamashita, and Y. Tsuchiya, ''Quantitation of absorbers in turbid media using time integrated spectroscopy based on microscopic Beer–Lambert law,'' *Jpn. J. Appl. Phys., Part 1* **37**(5A), 2724–2727 (1998).
21. H. Zhang, Y. Tsuchiya, M. Miwa, T. Urakami, and Y. Yamashita, ''Time integrated spectroscopy of turbid media based on microscopic Beer–Lambert law: consideration of the wavelength dependence of scattering properties,'' *Opt. Commun.* **153**, 314–322 (1998).
22. H. Zhang and Y. Tsuchiya, ''Time integrated spectroscopy of turbid media based on the microscopic Beer–Lambert law: application to curved boundaries'' (unpublished).
23. H. Zhang, M. Miwa, T. Urakami, Y. Yamashita, and Y. Tsuchiya, ''Simple subtraction method for determining the mean pathlength traveled by photons in turbid media,'' *Jpn. J. Appl. Phys., Part 1* **37**(2), 700–704 (1998).
24. H. J. van Staveren, C. J. M. Moes, J. van Marle, S. S. Prahl, and M. J. C. van Gemert, ''Light scattering in Intralipid-10% in the wavelength range of 400–1100 nm,'' *Appl. Opt.* **30**(31), 4507–4514 (1991).
25. S. J. Matcher, M. Cope, and D. T. Delpy, ''*In vivo* measurements of the wavelength dependence of tissue-scattering coefficients between 760 and 900 nm measured with time-resolved spectroscopy,'' *Appl. Opt.* **36**(1), 386–396 (1997).